LBL-25584
Preprint

Lawrence Berkeley Laboratory
UNIVERSITY OF CALIFORNIA

Materials & Chemical Sciences Division

Submitted to Journal of the Electrochemical Society

Effects of Finite Rates of a Homogeneous Reaction on the Dissolution of Copper in Chloride Solutions

A.K. Hauser and J. Newman

July 1988

Prepared for the U.S. Department of Energy under Contract Number DE-AC03-76SF00098.

DISCLAIMER

LBL-25584

Effects of Finite Rates of a Homogeneous Reaction on the Dissolution of Copper in Chloride Solutions

Alan K. Hauser and John Newman

Materials and Chemical Sciences Division, Lawrence Berkeley Laboratory,
and Department of Chemical Engineering, University of California,
Berkeley, CA 94720

July 28, 1988

Abstract

The steady-state dissolution of a copper rotating disk in 0.1 N HCl is investigated. Specifically, the effect of finite rates of the homogeneous complexing reaction is explored by utilizing a perturbation analysis. Formulating the singular perturbation problem leads to a better understanding of the physical nature of the system and enables one to characterize quantitatively the numerical errors resulting from the Stefan-Maxwell algorithm that arise for certain values of the rate constants. Additionally, a new way of plotting the steady-state polarization behavior is introduced that reduces the number of independent parameters of the system to a minimum. Concentration and potential profiles as functions of distance from the electrode, calculated using a macroscopic model based on concentrated-solution theory and Butler-Volmer kinetics, are interpreted by means of the perturbation analysis.

---

key words: rotating disk, singular perturbation, steady-state profiles, polarization behavior, complexing

1. Introduction

A mathematical treatment of the steady-state polarization characteristics of a rotating disk electrode is to be presented. The Stefan-Maxwell model discussed earlier[1] has been used to predict the concentration and potential profiles, as well as the current-potential behavior, for the largely mass-transfer controlled anodic dissolution of copper in chloride solutions[2] written as

$$Cu \rightarrow Cu^{+} + e^{-} \quad . \tag{1}$$

The effect of finite rates of the homogeneous reaction

$$Cu^{+} + 2Cl^{-} \rightarrow CuCl_{2}^{-} \tag{2}$$

has been investigated over a wide range of rate constants for this reaction. However, for certain combinations of values of the equilibrium and kinetic constants, numerical difficulties arise because concentration gradients become steep and finite-difference approximations lose accuracy. Thus, a perturbation technique is used as a guide for understanding the physical nature of the problem. For example, the perturbation solution indicates sources of error in the computer formulation and may be used to estimate the order of magnitude of these errors.

Before proceeding with the mathematical treatment, let us briefly discuss the electrochemistry that gives rise to such an analysis. A singular perturbation problem arises when the homogeneous-reaction rate constant is large enough to allow the diffusion boundary layer to be treated as two regions: (i) the homogeneous reaction zone, where the concentrations are distributed according to the rate of the complexing reaction, and (ii) the remainder of the diffusion layer, where the concentration profiles are determined by the equilibrated homogeneous reaction.

We will present a rigorous justification of the separation of the electrolytic solution into two regions by means of a singular-perturbation expansion of the concentration.[3] A singular perturbation consists of two perturbation expansions valid respectively in the region away from the interface and close to the interface. Since they describe the same function, the two expansions must match in an intermediate region. In other words, the outer limit of the inner concentration expansion agrees, to all orders in the perturbation parameter and the distance variable, with the inner limit of the outer expansion. Again, the reason for constructing two such perturbation expansions is that different approximations are valid in the two regions. In the outer region of the diffusion-boundary layer, one can neglect departures from equilibrium of the chemical complexing reactions assuming infinitely fast equilibration as a first approximation, so only diffusion and convection need to be accounted for. In the inner region (near the interface) convection can be neglected, but it is necessary to consider the finite rates of the homogeneous reactions as well as diffusion. For the perturbation analysis, migration is assumed to be negligible in both regions because of the excess of supporting electrolyte that is present.

2. Perturbation Formulation

The governing equations and boundary conditions, using dilute-solution theory with no migration, are presented here for the steady-state dissolution of copper in chloride solutions. The minor species, Cu^+ and $CuCl_2^-$, are treated in an excess of supporting electrolyte, *i.e.*, HCl, such that the chloride concentration can be taken to be constant. Thus, the material balances are given as follows

$$v_z \frac{dc_3}{dz} = D_3 \frac{d^2c_3}{dz^2} + \hat{k}_b(c_4 - \hat{K}^* c_3) \tag{3}$$

$$v_z \frac{dc_4}{dz} = D_4 \frac{d^2c_4}{dz^2} - \hat{k}_b(c_4 - \hat{K}^* c_3) \quad , \tag{4}$$

where 3 and 4 represent Cu^+ and $CuCl_2^-$, respectively. In this analysis for large Schmidt numbers, the axial velocity profile is given by[4]

$$v_z = -a\Omega \left(\frac{\Omega}{\nu}\right)^{1/2} z^2 \quad , \tag{5}$$

where Ω is the angular rotation speed, ν is the kinematic viscosity, and $a = 0.51023262$.

The boundary conditions in the bulk are

$$c_i = c_{i,\infty} \quad \text{and} \quad \Phi = 0 \quad \text{at} \quad z = z_{\max} \quad , \tag{6}$$

where the arbitrary zero of potential is specified at

$$z_{\max} = 2.0 \left(\frac{3D_{\max}}{a\nu}\right)^{1/3} \left(\frac{\nu}{\Omega}\right)^{1/2} \quad , \tag{7}$$

and the problem is scaled using the largest diffusion coefficient $D_{\max}$. The boundary condition at the electrode relates the flux of species i to the electrochemical reaction occurring at the surface

$$N_i = -D_i \frac{dc_i}{dz} = -\frac{s_i}{nF} i_n \quad , \tag{8}$$

where s_i is the stoichiometric coefficient of species i, n is the number of electrons transferred in the single electrode reaction, and i_n is the normal component of the faradaic current density.

2.1. Governing Equations for the Outer Solution Region

The modified homogeneous-reaction equilibrium relationship

$$\hat{K}^* = \frac{\hat{k}_f^*}{\hat{k}_b} = \frac{c_4}{c_3} \tag{9}$$

is applicable because the complexing-reaction backward rate constant $\hat{k}_b$ is large, and the chloride concentration is taken to be constant due to the presence of an excess of HCl. Addition of equations 3 and 4 yields

$$v_z \frac{d(c_3 + c_4)}{dz} = \frac{d^2(D_3 c_3 + D_4 c_4)}{dz^2} \quad . \tag{10}$$

Substitution of equation 9, with rearrangement, gives

$$v_z \frac{dc_4}{dz} = D \frac{d^2 c_4}{dz^2} \quad , \tag{11}$$

where the effective diffusion coefficient is given by

$$D = \frac{D_3 + \hat{K}^* D_4}{1 + \hat{K}^*} \quad . \tag{12}$$

Equation 11 is a first-order differential equation for dc_4/dz and can be integrated twice to give the well-known solution[5] in the high-Schmidt-number approximation

$$c_4 = \hat{K}^* c_3 = A \, i_n \int_{\xi}^{\infty} e^{-\chi^3} \, d\chi \quad , \tag{13}$$

where A is an integration constant to be given later. The rotating-disk problem is properly scaled using the dimensionless parameter

$$\xi = z \left(\frac{\Omega}{\nu} \right)^{1/2} \left(\frac{a\nu}{3D} \right)^{1/3} = \frac{z}{\delta} \quad , \tag{14}$$

which arises from the dimensionless convective-diffusion equation[5] and δ is the boundary-layer thickness. For small values of ξ, the concentrations of species 3 and 4

are given by

$$c_4 = \hat{K}^* c_3 = A\, i_n \left[\Gamma(4/3) - \xi\right] \quad , \tag{15}$$

although these concentration profiles do not reflect the differences between species 3 and 4 as required by stoichiometry of the reaction. Thus, equations 13 and 15 do not satisfy the boundary condition at the surface as given by equation 8. Let us next treat the region next to the electrode surface where the complexing reaction is not equilibrated, and finite rates of the homogeneous reaction must be accounted for.

2.2. Governing Equations for the Inner Solution Region

Convection can be ignored in the inner region close to the electrode surface; thus, equation 10, when using the dimensionless distance ξ, reduces to

$$\frac{d^2(D_3 c_3 + D_4 c_4)}{d\xi^2} = 0 \quad . \tag{16}$$

The solution to this equation is obtained by integrating twice to give

$$D_3 c_3 + D_4 c_4 = P + Q\xi \quad . \tag{17}$$

Matching with the inner limit of the outer solution (equation 15) enables P and Q to be related to $A\, i_n$ with the result

$$D_3 c_3 + D_4 c_4 = \left(\frac{D_3}{\hat{K}^*} + D_4\right) A\, i_n \left[\Gamma(4/3) - \xi\right] \quad . \tag{18}$$

By returning to the original governing equations, c_3 in equation 4 can be eliminated by using equation 18. When convection is neglected within the inner region, substitution and rearrangement of the material balance for species 4 yields the following equation

$$\frac{d^2 c_4}{d\xi^2} = \frac{1}{\Delta^2}\left[c_4 - A\, i_n\Big(\Gamma(4/3) - \xi\Big)\right] \quad , \tag{19}$$

where the dimensionless perturbation parameter Δ is given by

$$\Delta = \left(\frac{1}{\hat{k}_b \delta^2}\,\frac{D_3 D_4}{D_3 + \hat{K}^* D_4}\right)^{1/2} \quad . \tag{20}$$

The solution to this equation is

$$c_4 = \alpha_4 e^{\xi/\Delta} + \beta_4 e^{-\xi/\Delta} + A\, i_n\Big[\Gamma(4/3) - \xi\Big] \quad , \tag{21}$$

where $\alpha_4 = 0$ so that c_4 is bounded at infinity. Since $dc_4/d\xi = 0$ at $\xi = 0$ according to equation 8, $\beta_4 = -A\, i_n \Delta$.

Equation 18 yields c_3 as follows

$$c_3 = A\, i_n \Delta \frac{D_4}{D_3}\, e^{-\xi/\Delta} + \frac{A i_n}{\hat{K}^*}\Big[\Gamma(4/3) - \xi\Big] \, , \tag{22}$$

upon substitution of equation 21 for c_4. Next, the boundary condition at $\xi = 0$, given by equation 8 for species 3, enables the constant A in equation 22 to be determined

$$A = \frac{\delta/F}{D_3/\hat{K}^* + D_4} \quad . \tag{23}$$

Finally, the concentrations of species 3 and 4 at the surface are given by

$$\frac{c_{3,0}}{i_n} = \frac{\delta}{F D_3}\,\frac{D_3\Gamma(4/3) + \Delta D_4 \hat{K}^*}{D_3 + D_4 \hat{K}^*} \quad , \qquad \frac{c_{4,0}}{i_n} = \frac{\delta \hat{K}^*}{F}\,\frac{\Gamma(4/3) - \Delta}{D_3 + D_4 \hat{K}^*} \quad , \tag{24}$$

respectively.

2.3. Composite Solution

We have constructed two expansions, *e.g.*, equations 13 and 21 for c_4, which are valid in different, but overlapping regions of ξ, and these two expansions match in the region of overlap. The expansion, valid for all values of ξ, is obtained by adding the

inner and outer solutions, followed by subtracting the terms common to both the inner and outer expansions. Thus, the "composite expansions" for the concentrations of species 3 and 4 as a function of the dimensionless distance from the electrode are as follows

$$c_3(\xi) = \frac{i_n}{F} \frac{\delta}{D_3 + D_4 \hat{K}^*} \left[\int_{\xi}^{\infty} e^{-\chi^3} \, d\chi + \Delta \hat{K}^* \frac{D_4}{D_3} \, e^{-\xi/\Delta} \right] \tag{25}$$

$$c_4(\xi) = \frac{i_n}{F} \frac{\delta \hat{K}^*}{D_3 + D_4 \hat{K}^*} \left[\int_{\xi}^{\infty} e^{-\chi^3} \, d\chi - \Delta \, e^{-\xi/\Delta} \right] . \tag{26}$$

2.4. Polarization Behavior

The current is related to the potential by the modified Butler-Volmer equation

$$i_n = F k_a \exp\left[\frac{(1-\beta)F}{RT} \, V \right] - F k_c c_{3,0} \exp\left[-\frac{\beta F}{RT} \, V \right] . \tag{27}$$

Substitution of equation 24 for $c_{3,0}$, with rearrangement, yields

$$i_n = \frac{F k_a \exp\left[\frac{(1-\beta)F}{RT} \, V \right]}{1 + k_c \frac{\delta}{D_3} \frac{D_3 \Gamma(4/3) + \Delta D_4 \hat{K}^*}{D_3 + D_4 \hat{K}^*} \exp\left[-\frac{\beta F}{RT} \, V \right]} . \tag{28}$$

For the fast electrode kinetics of the copper system, with the expected values of k_a, k_c, and V, the one in the denominator is negligible, as one would have obtained by using a Nernst equation. With this simplification, equation 28 can be written as

$$\frac{i_n}{F} \frac{k_c}{k_a} \frac{\delta}{D} \frac{\Gamma(4/3)}{\exp(FV/RT)} = \frac{D_3 \Gamma(4/3) \, [\, 1 + \hat{K}^* \,]}{D_3 \Gamma(4/3) + \Delta D_4 \hat{K}^*} , \tag{29}$$

a form which suggests a general correlation of the current-potential curve.

3. Results

Steady-state results are presented here for the electrodissolution of copper in chloride solutions. Unless specified otherwise, all cases are for a copper disk rotating at 2000 rpm in 0.1 N HCl with a kinetic viscosity of $\nu = 8.9 \times 10^{-3}$ cm^2/s. The kinetic and thermodynamic input parameters are summarized in table 1 for the two-step copper dissolution mechanism given by equations 1 and 2. The potential between the working and saturated calomel reference electrode is $V = -0.205$ V.

The concentration profiles of the minor species, as calculated by the Stefan-Maxwell macroscopic model,[1] are given in figures 1 and 2, where the dimensionless concentrations are normalized with respect to the resulting current density. Figure 1 illustrates cuprous ion profiles as a function of the dimensionless distance ξ from the anode for three values of the homogeneous complexing-reaction rate constant, $\hat{k}_b = 0\ \text{s}^{-1}$, $10^{-2}\ \text{s}^{-1}$,and $10^{0}\ \text{s}^{-1}$. With no homogeneous reaction, the cuprous ion

Table 1. Model input parameters for the dissolution of copper in 0.1 N HCl.

$k_a = 10^{-5}$ mol/cm^2·s	$k_c = 70$ cm/s
$\hat{K}^* = \hat{K}_c c^2_{\text{Cl}^-,\infty} = 695$	$\hat{k}_b = 0,\ 10^{-2},\ 10^{0},\ 10^{2},\ 10^{4},\ \infty\ \text{s}^{-1}$
$D_3 = 0.72 \times 10^{-5}$ cm^2/s	$D_4 = 0.568 \times 10^{-5}$ cm^2/s
$D_{\text{max}} = 9.31 \times 10^{-5}$ cm^2/s (for H^+)	$D_{\text{Cl}^-} = 2.03 \times 10^{-5}$ cm^2/s

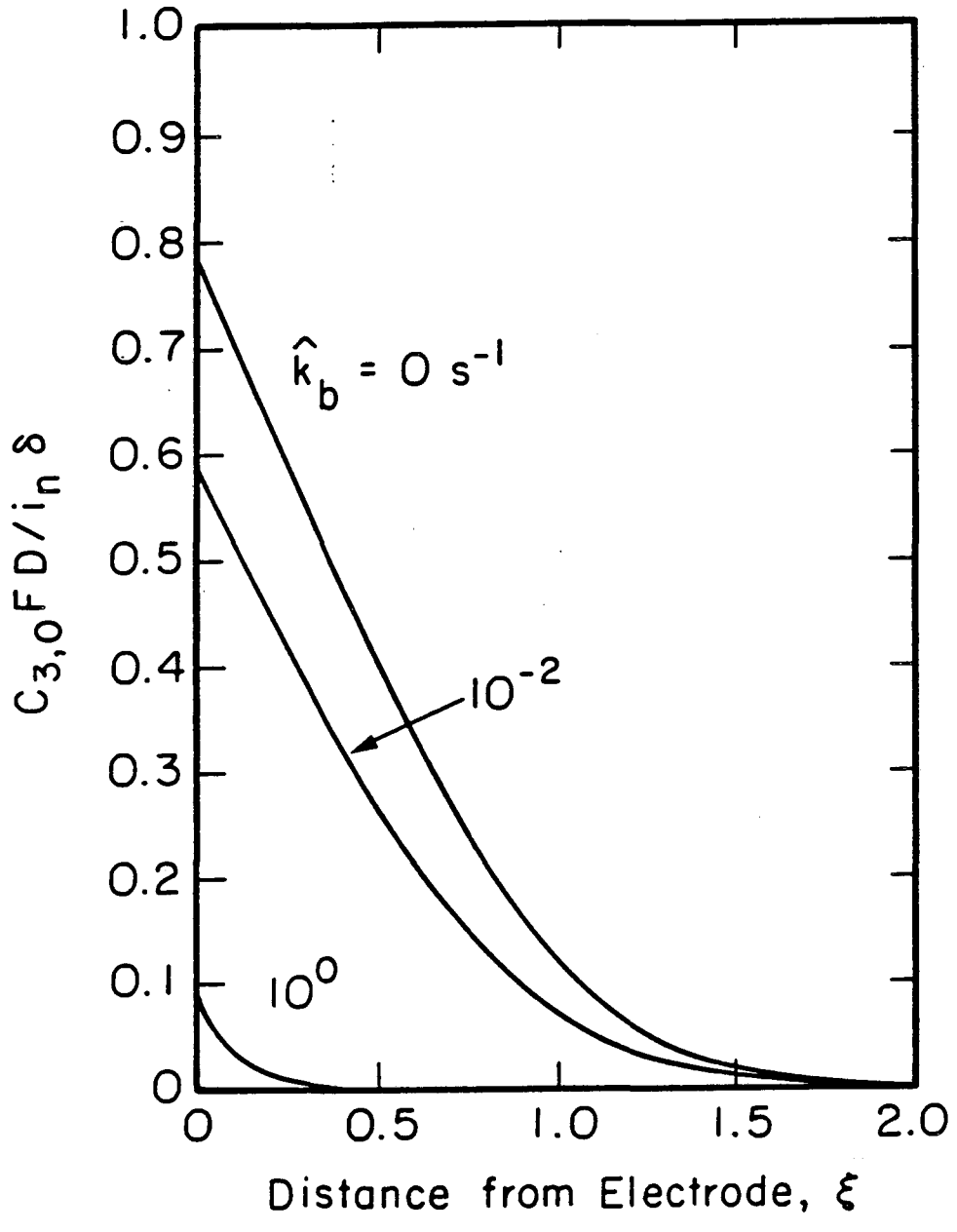

Figure 1. Dimensionless cuprous concentration profiles as a function of the dimensionless distance ξ from the disk electrode ($V = -0.205$ V and $\Omega = 2000$ rpm).

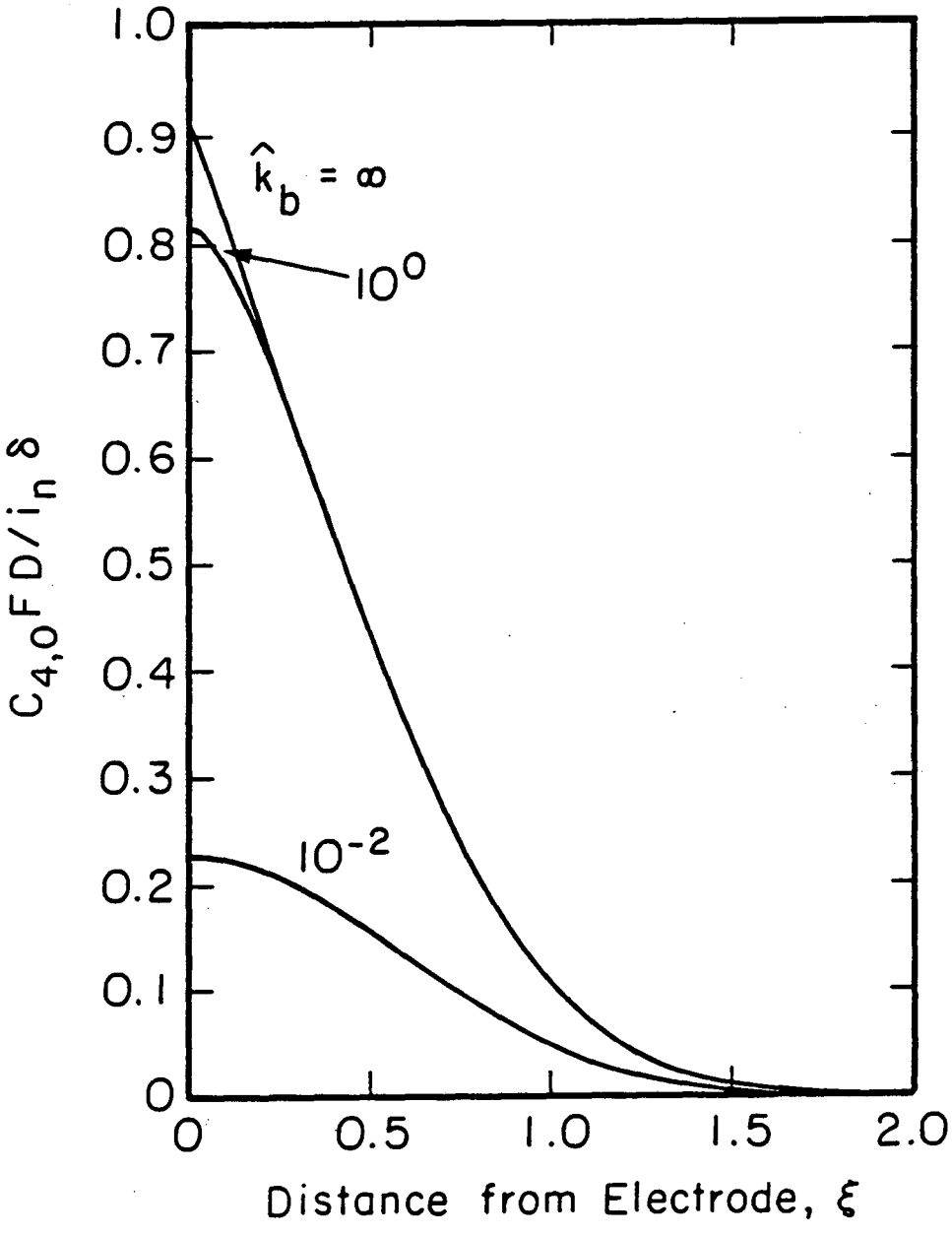

Figure 2. Dimensionless $CuCl_2^-$ ion concentration profiles as a function of dimensionless distance from the disk electrode ($V = -0.205$ V and $\Omega = 2000$ rpm).

concentration at the surface is given by $c_{3,0}/i_n = \overline{\delta}_3/F{\cdot}D_3$ according to equation 8, where the Nernst diffusion-layer thickness, $\overline{\delta}_3 = \Gamma(4/3)\delta_3$, corresponds to $\xi = \Gamma(4/3)\left(D_3/D\right)^{1/3} = 0.966$ in the figure. In this limiting case, reaction 1 occurs alone so that no $CuCl_2^-$ is formed, and the dimensionless cuprous concentration is a maximum. For larger values of $\hat{k}_b$, the ordinate of figure 1, $c_3FD/i_n{\cdot}\delta$, decreases because the current increases and the cuprous ion concentration remains constant ($c_{3,0} = 4.9 \times 10^{-11}$ mol/cm^3 for all $\hat{k}_b$ for the chosen value of V). This is a result of fast copper kinetics and Nernst-like behavior yielding a potential-controlled cuprous ion concentration. As $\hat{k}_b$ increases, the dimensionless concentration of the copper chloride complex is shown to increase, as expected, in figure 2. For large homogeneous rate constants ($\hat{k}_b > 10^{-2}$ s^{-1}), the concentration of the copper chloride complex c_4 is greater than the cuprous ion concentration. This trend is reversed for the $\hat{k}_b = 10^{-2}$ s^{-1} case shown in the two figures.

Because $CuCl_2^-$ does not participate in the electrochemical reaction, the slope of the curves in figure 2 are zero at $\xi = 0$ for finite values of $\hat{k}_b$. An infinitely large complexing rate constant enables reactions 1 and 2 to be combined as

$$Cu + 2Cl^- \longrightarrow CuCl_2^- + e^- \quad , \tag{30}$$

where the concentration given by equation 24 with $\Delta = 0$, $c_{4,0}/i_n = \overline{\delta}\hat{K}^*/F{\cdot}D{\cdot}(1+\hat{K}^*)$, is the upper limit shown in figure 2. The Nernst boundary-layer thickness, $\overline{\delta}$, corresponds to $\xi = 0.893$ for this reaction. The $\hat{k}_b = 10^4$ s^{-1} and infinity cases are indistinguishable in this figure, except for their slopes at $\xi = 0$; the infinite $\hat{k}_b$ case has a finite slope due to the electroactive $CuCl_2^-$, whereas the finite rate-constant case has a zero slope. The corresponding equilibrium amount of

cuprous ion, $c_3 = c_4/\hat{K}^*$, is so small for this infinitely fast rate of the complexing reaction that its profile cannot be seen in figure 1.

Next, we should like to compare the Stefan-Maxwell results with those from the perturbation analysis. The numerically calculated results (321 mesh points) are tabulated in parenthesis in table 2, where values in the last column of the table are calculated based upon reaction 30, for an infinitely fast complexing rate constant, as opposed to the two-step reaction mechanism. The kinetic expression

$$i_n = F k_a' c_{Cl^-,\infty}^2 \exp\left(\frac{(1-\beta)F}{RT} V\right) - F k_c' c_{4,0} \exp\left(-\frac{\beta F}{RT} V\right) \tag{31}$$

is applicable for $\hat{k}_b = \infty$, assuming the chloride ion concentration does not vary. The rate constants for this case are modified to be more consistent† with the two-step mechanism. Thus, $k_a' = k_a/c_{Cl^-,\infty}^2 = 10^3$ cm^4/mol·s and $k_c' = k_c/\hat{K}^* = 10^{-1}$ cm/s. Making these substitutions into equation 31 yields the original kinetic expression given by equation 27.

In table 2, the current densities and the surface concentrations, normalized with respect to the current density, are calculated from the perturbation analysis using equations 29 and 24, respectively, for all cases except $\hat{k}_b = 0$ s^{-1}. For the latter asymptotic limit, the current density is given by

---

† It should be pointed out, however, that reaction 30 is not equivalent to the two-step process (equations 1 and 2) with $\hat{k}_b = \infty$ because the chloride reaction order is different in the two cases.

Table 2. Comparison of the numerical Stefan-Maxwell results with those from the analytic solution as a function of the homogeneous backward rate constant.

$\hat{k}_b$ (s^{-1})	0	10^{-2}	10^{0}	10^{2}	10^{4}	∞
Δ	∞	1.0	0.1	0.01	0.001	0
i_n ($\mu A/cm^2$)	0.0348	0.0335	0.3299	2.8842	12.776	20.642
	(0.0339)	(0.0452)	(0.3278)	(2.0242)	(2.742)	(20.222)
$\frac{c_{3,0}FD}{i_n\delta}$	0.7625	0.7918	0.0803	0.00919	0.00207	0.00128
	(0.7829)	(0.5858)	(0.0808)	(0.01309)	(0.00967)	(0.00132)
$\frac{c_{4,0}FD}{i_n\delta}$	0	−0.11	0.7915	0.8817	0.8907	0.8917
	(0)	(0.2236)	(0.8134)	(0.8985)	(0.9028)	(0.9148)
$c_{4,0}/c_{3,0}$	0	−0.14	9.85	95.96	429.65	695.28
	(0)	(0.382)	(10.06)	(68.63)	(93.40)	(695.28)

$$\frac{i_n}{F} = \frac{k_a \exp\left(\frac{\beta F}{RT} V\right)}{1 + \frac{\bar{\delta}_3}{D_3} k_c \exp\left(-\frac{(1-\beta)F}{RT} V\right)} \tag{32}$$

Small to moderate values of $\hat{k}_b$ are included in order to reveal the limit of applicability of the perturbation analysis. Concentration ratios are calculated using the following relation

$$\frac{c_{4,0}}{c_{3,0}} = \frac{\Gamma(4/3) - \Delta}{\Gamma(4/3)/\hat{K}^* + \Delta D_4/D_3} \quad , \tag{33}$$

even though these are negative for $\Delta > \Gamma(4/3)$.

Examination of the results in table 2 indicates that numerical inaccuracies in the Stefan-Maxwell model arise for large, but finite, rate constants of the homogeneous complexing reaction ($\hat{k}_b > 10^0\ s^{-1}$). For example, an error of a factor of 4.7 arises for the case of $\hat{k}_b = 10^4\ s^{-1}$. For small values of the rate constant ($\hat{k}_b < 10^{-1}\ s^{-1}$) equations 24, 29, and 33 begin to break down. Thus, the perturbation analysis is valid only for $\Delta << 1$.

The normalized potential profiles are given in figure 3, where the zero of potential is specified at $z_{max} = 5.15 \times 10^{-3}$ cm, corresponding to $\xi_{max} = 5.1$. Five different values of the homogeneous reaction backward rate constant $\hat{k}_b$ are given, and three distinct features are revealed. In all cases, the potential is determined by the magnitude of two different potentials: the ohmic potential drop and the diffusion potential. Ohm's law, $i_n = -\kappa \nabla \Phi$, is characterized by the linear portion of the curve far from the electrode surface, but the magnitude of the diffusion potential next to the disk dictates the detailed shape of the potential profile.

For $\hat{k}_b = 0\ s^{-1}$, the potential profile is linear, except where deviations from Ohm's law occur close to the electrode surface. In the other asymptotic limit of $\hat{k}_b = \infty$, a maximum in the potential profile occurs, where the diffusion potential balances the Ohm's law portion of the curve and then determines the potential profile next to the surface. This behavior, where the electric field in the solution is reversed, has been shown[6] to occur for a number of different electrochemical systems and will be discussed

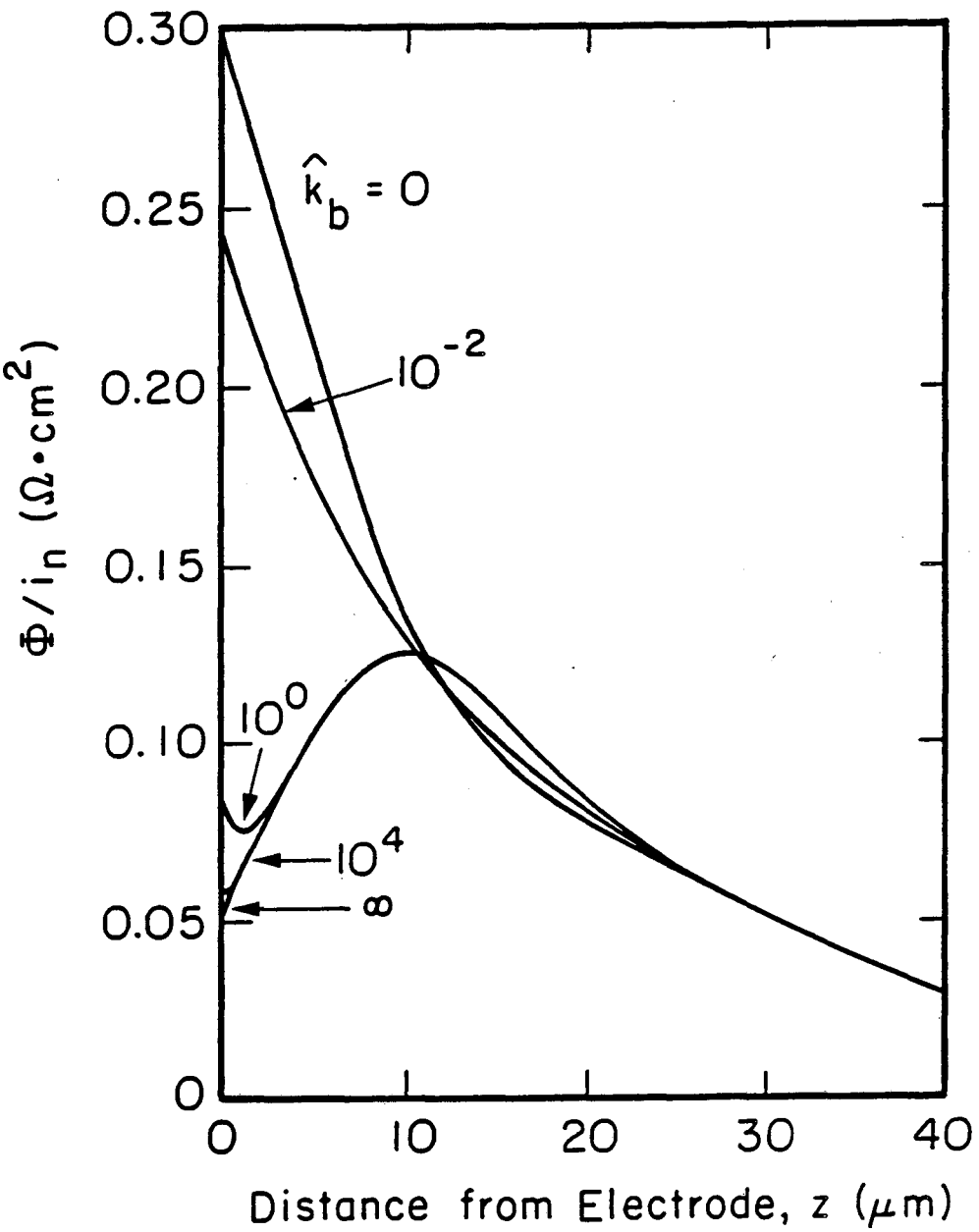

Figure 3. Normalized potential profiles as a function of distance from the disk electrode ($V = -0.205$ V and $\Omega = 2000$ rpm).

only briefly here.

At the electrode surface, the normal current flow can be shown[7] to be related to the potential gradient by

$$i_n = \frac{F^2}{RT} \frac{\sum_i z_i^2 c_i}{\sum_i \frac{z_i s_i}{n D_i}} \left(\frac{\partial \Phi}{\partial z} \right)_{z=0} \tag{34}$$

The stoichiometric coefficients, charge numbers, and magnitude of diffusion coefficients of the species participating in a particular reaction determine whether a potential maximum/minimum occurs or not. For example, the sum in the denominator in equation 34 is positive (or slope of figure 3 $= [d\Phi/z]/i_n = 103\ \Omega\cdot$cm for reaction 30) which implies that the potential gradient is reversed in comparison to Ohm's law. Equation 34 indicates reversal at the surface is not possible for reaction 1, since the denominator is negative (slope $= -185\ \Omega\cdot$cm). For intermediate values of $\hat{k}_b$ and $c_{4,0}/c_{3,0} > 1$, the salient features of both the asymptotic limits are displayed yielding both a minimum and a maximum in the potential. For $\hat{k}_b = 10^{-2}\ \mathrm{s}^{-1}$ ($c_{4,0}/c_{3,0} < 1$), neither a minimum nor maximum occurs within the boundary layer, similar to the $\hat{k}_b = 0\ \mathrm{s}^{-1}$ case. The slope at the surface remains at $-185\ \Omega\cdot$cm for each of these cases.

Steady-state polarization curves, as calculated from the perturbation analysis (valid asymptotically in the limit of small Δ), are given in figure 4 for different values of the homogeneous rate constant $\hat{k}_b$. Results for two different rotation rates, $\Omega = 1000$ and 2000 rpm, are given for the larger values of $\hat{k}_b$.

A dimensionless polarization curve is presented in figure 5 that is based on equation 29. This way of plotting the current-potential behavior is convenient for

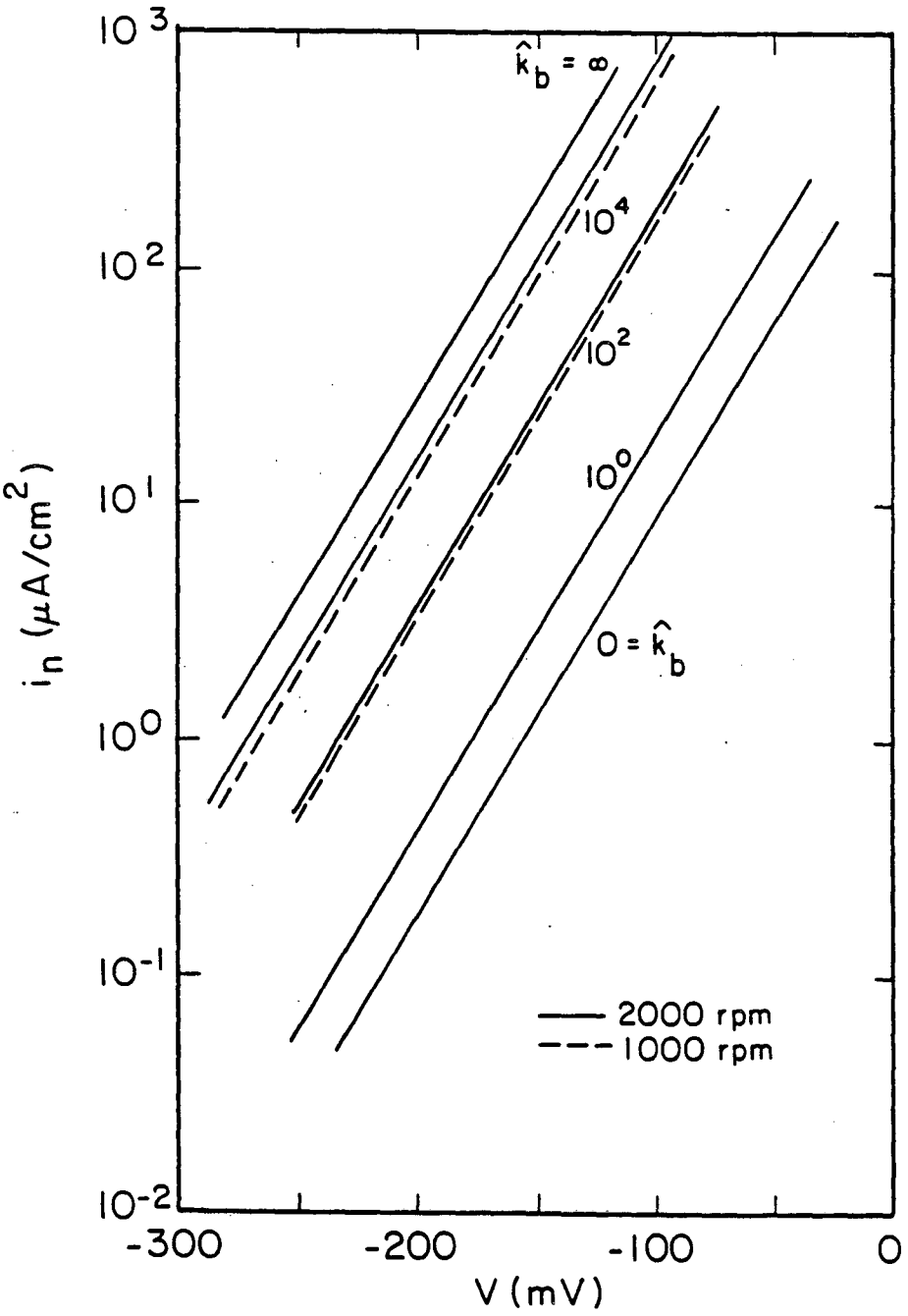

Figure 4. Steady-state polarization curves as a function of $\hat{k}_b$ and rotation speed.

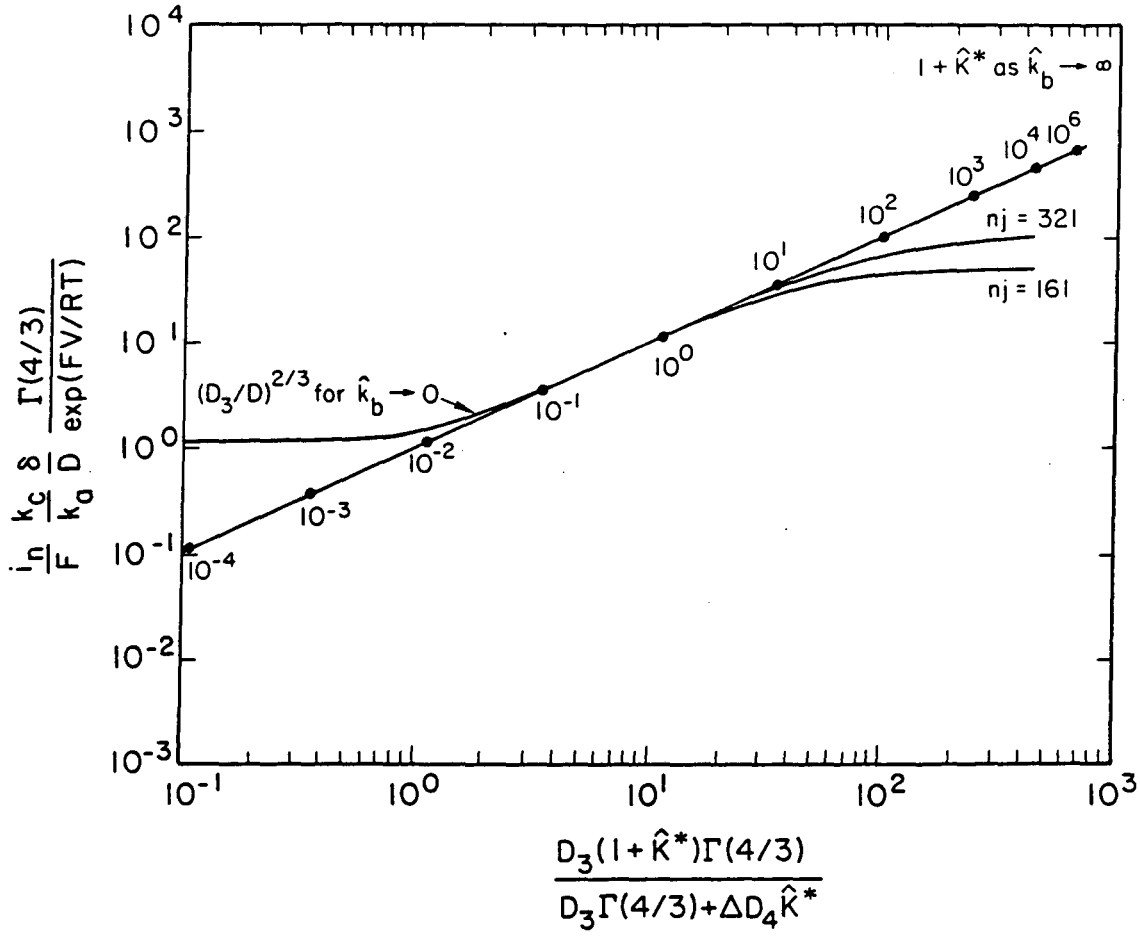

Figure 5. Dimensionless correlation of steady-state polarization behavior displaying the dependence on $\hat{k}_b$.

reducing the homogeneous-reaction rate constant and potential dependence to approximately one curve. Also shown on this plot are the numerically calculated Stefan-Maxwell results. Both 161 and 321 mesh-point results are plotted. Again, the numerical solution for large values of $\hat{k}_b$ is not good. As the homogeneous rate constant goes to zero, the left side of equation 29 should approach $(D_3/D)^{2/3}$ because the $\overline{\delta}_3/D_3$ term in equation 32 ($\hat{k}_b = 0\ s^{-1}$) is proportional to $D_3^{2/3}$. In the other limit of $\hat{k}_b \rightarrow \infty$ for which the perturbation analysis is valid, equation 29 goes to $1 + \hat{K}^*$.

This particular plot tends to eliminate substantial variations in current-potential curves (figure 4) due to variations in the rotation speed and potential V, and it displays the substantial dependence on $\hat{k}_b$. Thus, different values of k_c/k_a could be used to compensate for different values of $\hat{k}_b$, with equally good fits of the data. Calculated points can fail to fall on a single curve for several reasons, and the fact that they fall nearly on a single curve indicates that these factors are valid or can be ignored to a good approximation.

1. A single curve is spoiled when the one in the denominator of equation 28 cannot be ignored. However, the Nernst approximation is good in virtually all cases plotted.

2. Numerical (Stefan-Maxwell) results include effects of migration and variations of Cl^- concentration as well as interdiffusion effects. The closeness to a single curve indicates that these effects are of minor importance for the conditions reported here.

3. For moderate to low $\hat{k}_b$ values, the singular-perturbation analysis does not apply, and at $\hat{k}_b = 0\ s^{-1}$, the ordinate value should reach a limit while the abscissa value moves one off the graph toward infinity at the left. Results may still fortuitously fall on a single curve.

4. For high $\hat{k}_b$ values, the numerical (SM) calculations break down, and one cannot assess whether migration and variations of the chloride concentration and interdiffusion effects are truly negligible, although one can surmise from separate estimates that they do not become important unless currents are large.

4. Discussion of Results

The dimensionless perturbation parameter Δ, given by equation 20, characterizes the homogeneous reaction zone next to the electrode surface. In table 3, values of Δ are given as a function of the homogeneous rate constant $\hat{k}_b$. Also, values of the dimensional distance, z_Δ, corresponding to $\xi = \Delta$,

Table 3. Comparison of different perturbation parameters that characterize the homogeneous backward rate constant.

	Homogeneous rate constant, $\hat{k}_b$ (s^{-1})		
	10^0	10^2	10^4
Δ	0.1	0.01	0.001
z_Δ (cm)	1.0×10^{-4}	1.0×10^{-5}	1.0×10^{-6}
$\hat{\delta}_f$ (cm)	9.0×10^{-5}	9.0×10^{-6}	9.0×10^{-7}
$\hat{\delta}_b$ (cm)	2.4×10^{-3}	2.4×10^{-4}	2.4×10^{-5}

$$z_\Delta = \left(\frac{D_3 D_4 / \hat{k}_b}{D_3 + \hat{K} D_4} \right)^{1/2} , \tag{35}$$

are included in the table and can be used to judge the region of importance of homogeneous reaction in figure 3.

Δ represents a ratio of the penetration depth to a length characteristic of the thickness of the diffusion layer. The Nernst diffusion boundary layer thickness is given by $\overline{\delta} = 1.6117 \nu^{1/6} D^{1/3} \Omega^{-1/2} = 9.0 \times 10^{-4}$ cm, for the conditions reported in this paper. If the two characteristic lengths are of the same magnitude [$\Delta = O(1)$], then the finite rate of the homogeneous reaction must be accounted for in the region where convection is important. The computer program can handle this case easily and accurately. This was demonstrated for $\hat{k}_b \leq 10^0$ s^{-1}, and $\Delta \geq 0.1$.

For very small values of Δ (a fast homogeneous reaction or very large $\hat{k}_b$), equilibration of the homogeneous reaction could be assumed almost everywhere, and the two-step mechanism reduces (except chloride reaction order) to the one-step reaction 30. For the case of large, but finite $\hat{k}_b$, numerical inaccuracies arise because the concentration variations occur in such a small region next to the electrode surface. For example, this results when $\hat{k}_b = 10^4$ s^{-1} and $\Delta = 0.001$. In order to investigate the case for large values of the backward rate constants, a perturbation expansion accounting for the finite chemical reaction zone next to the electrode is necessary.

Finally, Δ should be compared with another dimensionless ratio $\hat{\delta}_b / \overline{\delta}$, where $\hat{\delta}_b$ is the homogeneous reaction thickness given by Levich[4] as $\sqrt{D/\hat{k}_b}$. Values of this parameter are included in table 3 and should be compared to the position next to the electrode in figure 3 where the minima occur. Because the correlation is not good,

values of $\hat{\delta}_f = \sqrt{D/\hat{k}_f^*}$ are also included in the table. It can be concluded that the perturbation parameters Δ and $\hat{\delta}_f$ are the most appropriate quantities for characterizing finite rates of the homogeneous reaction.

5. Conclusions

The generalized Stefan-Maxwell program[1] accounting for multicomponent diffusion, migration, and convection, in addition to any number of homogeneous and heterogeneous reactions, is a very powerful algorithm for studying many reaction mechanisms at a rotating disk. However, when utilizing computer implemented techniques, one must be cautious of numerical inaccuracies that can arise for certain values of the system parameters.

In this paper, the dissolution of a copper rotating disk has been studied. We have shown that a perturbation analysis for large, but finite, rates of the homogeneous complexing reaction is most helpful for elucidating numerical (SM) errors that did occur for these conditions. Additionally, the analytic solutions to the simplified governing equations (dilute-solution theory with no migration) help verify the unexpected potential profiles. Asymptotic limits for values of the homogeneous rate constant were presented and provided a window for studying the finite-rate cases. Finally, the perturbation analysis led to a simplified correlation (equation 29) for the entire current-potential curve. This new way of plotting the steady-state polarization behavior reduces the number of independent parameters for the system to a minimum.

Acknowledgements

This work was supported by the Assistant Secretary for Conservation and Renewable Energy, Office of Energy Storage and Distribution of the U.S. Department of Energy under Contract DE–AC03–76SF00098.

List of Symbols

a	0.51023
A	integration constant given by equation 22
c_i	concentration of species i, mol/cm^3
$c_{i,0}$	concentration of species i at the electrode surface, mol/cm^3
$c_{i,\infty}$	bulk concentration of species i, mol/cm^3
D_i	dilute-solution diffusion coefficient of species i, cm^2/s
D	effective diffusion coefficient, cm^2/s
e^-	symbol for the electron
F	Faraday's constant, 96,487 C/equiv
i_n	normal current density, A/cm^2
k_a	anodic rate constant for the electrochemical reaction, mol/cm^2·s
k_c	cathodic rate constant for the heterogeneous electrochemical reaction, cm/s
k_a'	anodic rate constant for the electrochemical reaction in the one-step mechanism, cm^4/mol·s
k_c'	cathodic rate constant for the heterogeneous electrochemical reaction in the one-step mechanism, cm/s
$\hat{k}_b$	backward rate constant for the homogeneous complexing reaction, 1/s
$\hat{k}_f^*$	modified forward rate constant for the homogeneous complexing reaction, 1/s

$\hat{K}_c$	concentration thermodynamic equilibrium constant for the homogeneous reaction, $cm^6/mol^2 \cdot s$
$\hat{K}^*$	thermodynamic equilibrium constant for the homogeneous complexing reaction
n	number of electrons involved in electrode reaction
N_i	molar flux of species i, $mol/cm^2 \cdot s$
P, Q	integration constants introduced in equation 17
R	universal gas constant, 8.3143 J/mol-K
s_i	stoichiometric coefficient of species i in the electrode reaction
T	absolute temperature, K
v_z	axial component of the velocity to a rotating disk
V	kinetic driving force (electrode potential relative to given reference electrode placed just outside double layer), V
z	normal distance from surface, cm
z_Δ	distance from electrode surface that best characterizes the homogeneous penetration depth, cm

Greek symbols:

α_4	constant in equation 21 for c_4
β_4	constant in equation 21 for c_4
β	symmetry factor
χ	dummy variable of integration
$\Gamma(4/3)$	0.89298, the gamma function of 4/3

δ	characteristic diffusion layer thickness, cm
$\overline{\delta}_i$	Nernst diffusion-layer thickness for species i, cm
$\hat{\delta}$	Levich homogeneous reaction penetration depth, cm
Δ	perturbation parameter given by equation 20
ν	kinematic viscosity, cm^2/s
ξ	dimensionless axial distance for rotating-disk convective-diffusion equation
Φ	electrostatic potential, V
Ω	angular rotation speed of disk, rad/s

subscripts:

a	anodic
b	backward reaction
c	cathodic
f	forward reaction
0	just outside the diffuse part of the double layer
∞	in the bulk electrolyte, where there are no concentration variations
3	cuprous ion
4	copper chloride complexed species

References

[1]. Alan K. Hauser and John Newman, "A Macroscopic-Impedance Model for a Rotating-Disk Electrode. I. Theoretical Treatment of the Electrochemical Impedance Using Concentrated-Solution Theory," to be submitted to *Journal of the Electrochemical Society,* (1988).

[2]. William H. Smyrl, "Electrochemistry and Corrosion on Homogeneous and Heterogeneous Metal Surfaces," *Comprehensive Treatise of Electrochemistry, 4,* Chapter 2, J. O'M. Bockris, Brian E. Conway, Ernest Yeager, and Ralph E. White, eds., New York: Plenum Publishing Corporation, 1981, pp. 97-149.

[3]. John Newman, "The Fundamental Principles of Current Distribution and Mass Transport in Electrochemical Cells," Allen J. Bard, ed., *Electroanalytical Chemistry* (New York: Marcel Dekker, Inc., 1973) *6,* 187-352.

[4]. Veniamin G. Levich, *Physical Hydrodynamics,* Prentice-Hall, Inc., Englewood Cliffs, N.J., (1962).

[5]. John Newman, *Electrochemical Systems,* Englewood Cliffs, N. J.: Prentice-Hall, Inc., 1973.

[6]. Alan K. Hauser and John Newman, "Electrolytic Mass Transfer to a Rotating Disk in Dilute Solutions: Concentration Variations of the Reacting, Excessive Supporting Electrolyte," Abstract 545, Spring ECS Meeting, Atlanta, 1988.

[7]. Alan K. Hauser and John Newman, "Potential and Concentration Variations of the Reacting, Supporting Electrolyte," submitted to *Journal of the Electrochemical Society.*

LAWRENCE BERKELEY LABORATORY
TECHNICAL INFORMATION DEPARTMENT
UNIVERSITY OF CALIFORNIA
BERKELEY, CALIFORNIA 94720